collides the long pulse laser light. The laser light can collide with about 200 micro-bunches. In this case, required timing stability is on the order of nanosecond or tens of nanoseconds. Thus, a system with a thermionic-cathode and Q-switch laser is most compact and can stably generate high flux X-rays with intention of 10^8 photons/s.

The idea of a laser pulse circulating system is based on multi-pulse laser-electron collision with laser circulation optics using a Pockels cell and a polarized beam splitter and multi-bunch electron beam from the thermionic cathode RF gun. After the first collision, laser light is turned on and reinjected into the CP. This system enhances the X-ray yield by a factor of 10 with 90% transmision efficiency of the circulation optics. To realize laser circulation optics for the intense laser pulse required for the X-ray source is challenging. Details of the laser pulse circulating system are discussed in §4.

2.2 *Requirement of beam energy*

Teh maximum energy of Compton scattered X-rays for head-on collisions depends on the wavelength (energy of photon) of the laser and the electron beam energy. The energy of the scattered photon k_s and the scattering angle of the photon $\cos\theta_s$ are derived from

$$k_s = \frac{(E_0 + P_0)k_0}{(1 + \cos\theta_s)k_0 + E_0 - P_0\cos\theta_s} \quad (1)$$

and

$$\cos\theta_s = \frac{k_s k_0 + E_0 k - (E_0 - P_0)k_0}{(P_0 - k_0)k_s}, \quad (2)$$

where k_0 is the energy of laser photon, P_0 and E_0 the momentum and energy of the electron beam, and θ_s the scattering angle of the photon ($\theta_s = 0$ for the direction of the electron beam).

Figure 4 indicates that requirement of beam energy for a 33.169 KeV X-ray is above 43.5 MeV for a Nd:YAG laser with a wavelength of 1064 nm.

2.3 *X-band linac*

The X-band linac is applied to the compact hard X-ray source. The RF-wavelength of the X-band (11.424 GHz) is 1/4 of the S-band (2.856 GHz). However, the maximum filed gradient of ~40 MV/m realizes remarkable compactness.

We designed a thermionic-cathode X-band RF gun and a

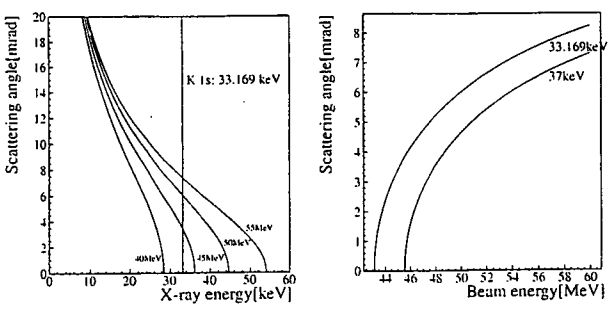

Fig. 4. Relation of beam energy and scattered photon for Nd:YAG laser (fundamental, 1064 nm) calculated using eq. (2). (a) Scattering angle of X-rays due to X-ray energy for each energy of the electron beam. (b) Scatteing angle due to beam energy for each X-ray energy.

Table II. Specifications for the X-band klystron modulator.

Output peak power	142 MW
Output voltage	500 kV
Output current	283 kA
Pulse length (FWHM)	3 μs
Flat top (±0.1%)	1 μs
Shot-by-shot fluctuation of pulse height	±0.1%
Repetition rate	50 pps
Average power	22 kW
Turn ratio of pulse transformer	1 : 32 (15.63 kV : 500 kV)
Size (PFN and control system)	1600 W × 2000 H × 1000 D
Size (with klystron)	3115 W × 2255 H × 1350 D

photo-cathode X-band RF gun. We carried out a fundamental design for the photo-cathode RF gun using the PARMALA code. Numerical analysis of the beam transport for the whole system including the photo-cathode X-band RF gun and X-band accelerating structure at the first stage has been presented.[6,7] The beam energy in this system reached 56.4 MeV.

A 3.6-cell thermionic-cathode X-band RF gun is being manufactured by Ishikawajima Harima Heavy Industry (IHI). Two 0.7 m long X-band accelerating structures are used for the X-ray source. The technology of the X-band accelerating structure developed for future linear colliders[8] at KEK and Stanford Linear Accelerator Center (SLAC) is fully adapted to this development. At first, the RDS (detuned) type accelerating structure has been adopted, which is already being manufactured by IHI.

We adopted a periodic permanent magnet (PPM) X-band klystron (Toshiba E3768I) designed for linear colliders. klystron modulator (poulsed power supply) was designed to fit this X-ray source. Specifications for the modulator are shown in Table II. A turn ratio of 1:32 is adopted for high voltage output with low voltage PFN to realize the small size of the main body.

The RF power is above 50 MW in a 1 μs pulse width.

2.4 *X-ray yield and properties*

The X-ray yield per bunch is calculated using,

$$N_{\text{X-ray}} = \sigma_{\text{Comp}}\mathcal{L} \quad (3)$$

where σ_{Comp} is the total cross section of Compton scattering that is calculated from the Klein–Nishina's formula,[9,10] and $\mathcal{L}$ is the luminosity of the laser-electron collision per bunch. For head-on collisions in which the velocity of each beam is $\sim c$, (integrated) luminosity per collision (bunch) $\mathcal{L}$ is written as:

$$\mathcal{L} = 2N_e N_l \int_{-\infty}^{\infty} \frac{1}{2\pi} \frac{1}{\sqrt{\sigma_{xe}^2(s) + \sigma_{xl}^2(s)}} \frac{1}{\sqrt{\sigma_{ye}^2(s) + \sigma_{yl}^2(s)}} \times \frac{1}{\sqrt{2\pi(\sigma_{se}^2 + \sigma_{sl}^2)}} \exp\left\{-\frac{(2s)^2}{2(\sigma_{se}^2 + \sigma_{sl}^2)}\right\} ds, \quad (4)$$

where N_e and N_l are numbers of electrons and laser photons, and $\sigma_{(x,y,s)(e,l)}$ is the rms beam size of the laser (l) and electron (e) beam for x, y (transverse) and s (longitudinal) axes. Beam profiles of both beams are assumed to be Gaussian. Luminosity is calculated by integrating eq. (4) numerically for the region (±0.5 m) between each focusing-

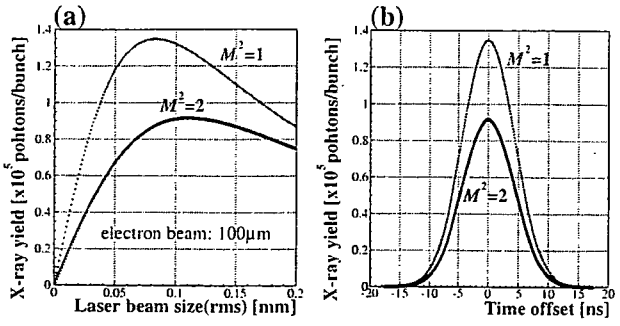

Fig. 5. (a) X-ray yield due to laser beam size for a single bunch and (b) X-ray yield of each bunch due to the time offset between the laser pulse and the electron beam bunch.

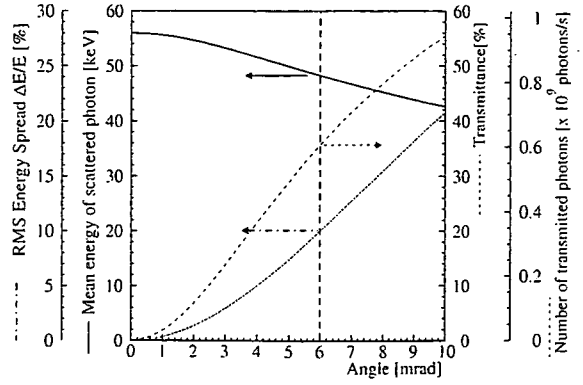

Fig. 7. Relation of collimated angle and the transmittance of photons, the number of photons transmitted (right axis), rms energy spread, and mean energy of the transmitted photons (left axis).

magnet of the electron beam upstream and down stream of the collision point that is large enough to be calculated with the Raylegh-length of laser light (0.11 m) and beta of the electron beam (0.1 m) at the CP.

We choose a stable system by focusing on only averaged X-ray flux. We construct the system with the thermionic-cathode RF gun (20 pC/bunch, $\sim 10^4$ bunches/RF-pulse, 10π mm·mrad) and the 2 J/pulse Q-switch Nd:YAG laser.

We adopt head-on collisions to achieve the maximum X-ray yield. Figure 5(a) indicates that optimal laser beam size is 82 μm (rms) for an electron beam size of 100 μm (rms) at the CP. Where M^2 (≥ 1) is difference of laser profile (quality) from ideal Gaussian. Each bunch collides with laser light at some time offset. The X-ray yield of each bunch is shown in Fig. 5(b). Thus, this system generates X-rays with 1.7×10^7 photons/pulse at $M^2 = 1$ (1.7×10^8 photons/s) that are the sum of all bunches. In $M^2 = 2$, the total X-ray yield is 0.9×10^7 (0.9×10^8 photons/s).

The total X-ray energy spectrum and the realtion of X-ray energy to scattering angle (for $M^2 = 1$) are shown in Fig. 6. The solid line indicates the X-ray energy spectrum calculated by the Klein–Nishina's formula and the luminosity calculation. The histogram in (a) shows the result of beam-beam interaction Monte-Carlo simulation code CAIN.[11] The maximum X-ray energy is 56 keV at a beam energy 56 MeV.

The energy of scatterd X-rays shown in Fig. 6(a) seems not narrow, but we can see the relation of the energy to the scattering angle in Fig. 6(b). That means the X-rays with higher energy can be chosen using a collimator. Figure 7 shows the relation of the scattering angle of transmitted photons at the collimator and the transmittance of photons, the number of photons transmitted (right axis), rms energy spread, and mean energy of transmitted photons (left axis) calculated by Klein–Nishina's eq. ($M^2 = 1$). It is assumed that the size of the light source is negligibly small. Figure 7 idicates that an energy spread of 10% of the rms is available at 36% transmittance for a 6 mrad scatterd angle of photon. Actually, 28% of total scatterd photon is available for application, because of the transmittance of of a 33 keV X-ray is approximately 80% at thin (1 mm) mirror to insident the laser light to the CP (Yoy can see the location of the mirror in Fig. 13). The attenuation of the X-rays at the thin (tens of μm) beryllium window that separates vacuum from air is negligibly small.

2.5 *Optimization of beam parameter at collison point*

The beam parameters at the CP is must be known to designs the beam line. The X-ray yield in a laser-electron collision depends on emittance, M^2, and Twiss (Courant–Snyder) parameters of the laser and the electron beam at the CP.

Figure 8 shows the maximum X-ray yield for each electron beam size at the CP. The laser spot is optimized to maximize the X-ray yield. A beam emittance of 10 mm·mrad for x and y axes is assumed to simplify the discussion. It is not effective to making the beam size less than 100 μm rms for an X-ray yield with a long pulse laser of 10 ns (FWHM).

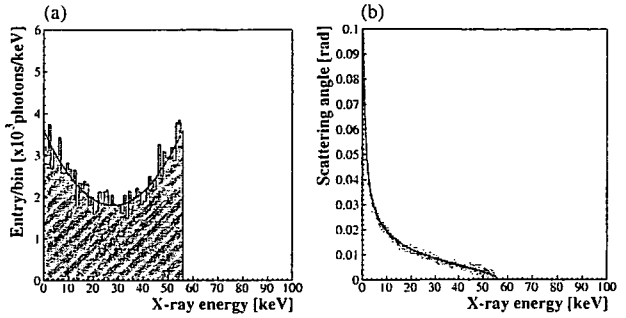

Fig. 6. (a) Total X-ray spectrum and (b) relation of X-ray energy and scattering angle of photon in single bunch (20 pC/bunch) collision with Q-switch Nd:YAG-laser (fundamental, 1064 nm).

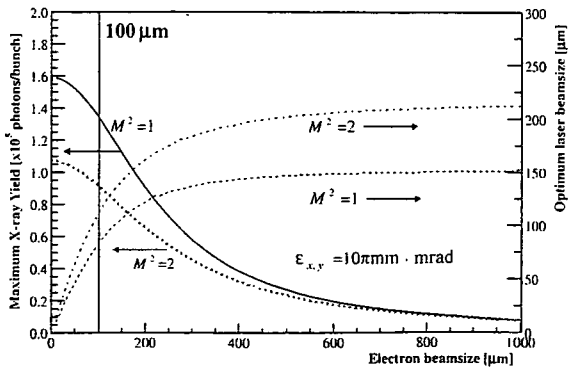

Fig. 8. Maximum X-ray yield and optimum laser size at the CP due to electron beam size at the CP for an electron emittance $\varepsilon_x = \varepsilon_y = 10\pi$ mm·mrad, and an electron charge of 20 pC/bunch.

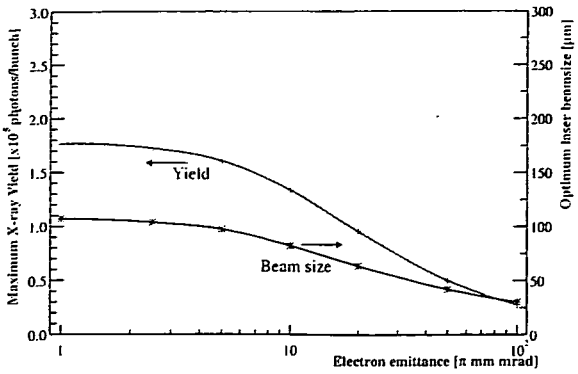

Fig. 9. Maximum X-ray yield and optimum laser size at the CP due to electron beam emittance.

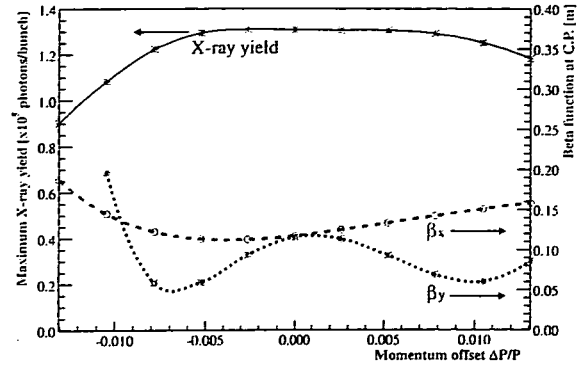

Fig. 11. The beta function (β_x, β_y) at the CP and X-ray yield due to momentum offset of the electron beam.

The maximum X-ray yield due to electron beam emittance with a beam size of 100 μm at the CP is indicated in Fig. 9. A very small beam emittance is not effective for X-ray yield because an emittance of 8.5×10^{-8} m·rad from a laser (with a wavelength of 1064 nm and $M^2 = 1$) is larger than an optical beam emittance of 1×10^{-8} m·rad (1π mm·mrad with 50 MeV).

2.6 Design of beam transport line

To prove that X-band beam acceleration and the generation of intense hard X-rays using an X-band system occurs, a beam transport line is designed using the SAD[12] program.

The first results of the numerical analysis for a thermionic-cathode X-band RF gun and the alpha-magnet are used to the design of the beamline as initial beam parameters.

Requirements for the beam line are: (1) a short beam line (<6 m between the alpha-magnet and CP), (2) the beam must bend 90 degrees to reduce the background signal for the X-rays, (3) a small dispersion and chromaticity at the CP to reduce fluctuations in X-ray intensity due to beam energy, (4) a small beam size of about 100 μm at the CP, and (5) a long drift space for the laser and the electron beam monitor around the CP.

The beam line designed using the SAD program is shown in Fig. 10. Beam tracking simulations with space charge effects using SAD also indicate that a 100 μm beam size at the CP is expected.

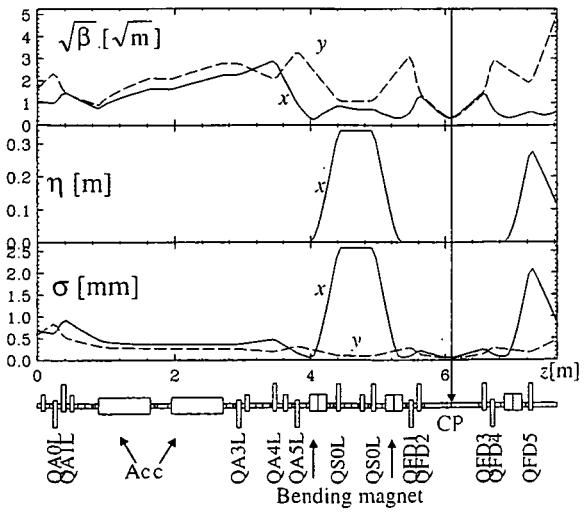

Fig. 10. Beam optics for compact hard X-ray source designed using SAD[10] program.

The effects of alignment/K-value error of the Q-magnets and bending magnets are estimated. Errors in the K-value, the transverse offset and tilt angle must be less than 0.1%, ±50 μm and 1 mrad (rms) to achive a small dispersion of less than 10 mm at the CP.

2.7 Shot-by-shot fluctuation of X-ray yield

Fluctuation of X-ray yield (luminosity) is caused by fluctuation in the parameters of the laser and electron beams at the C. P. Those of the electron depend mainly on the beam energy and the beam optics.

The beta function (β_x, β_y) at the CP and the X-ray yield due to the momentum offset of the electron beam are shown in Fig. 11. In the proposed system, the momentum of the electron beam depends on (1) the RF power input RF gun and accelerating structure (s), and (2) the difference between the RF phase and the length of the beam orbit between the RF gun and the accelerating structure. The momentum is independent of the RF phase shift in the klystron due to the klystron input voltage because RF gun and accelerating structure are driven by the same klystron. From the specifications of the klystron modulator shown in Table II, fluctuation in the beam momentum can be expected to ±0.125%.[13] With the X-ray yield due to beam momentum shown in Fig. 11, fluctuation in X-ray flux due to fluctuation of beam energy and chromaticity at the CP is less than 1%.

Fluctuation of the position and crossing angle of the laser and electron beams also depends on the beam energy and the dispersion functions η, η' at C. P. We expect that the small dispersion less than 10 mm are achieved by the dispersion correction technique. In this case, the position stability is about ±12.5 μm. Then the X-ray fluctuation due to momentum dispersion of electron beam optics may be ignored.

Typical fluctuations in laser energy of a Q-switch laser are ±2%. The fluctuation in X-ray yield about 50% r.m.s due to the micro structure in the temporal profile of the Q-switch Nd:YAG laser[14,15] is suppressed to less than 3.5% by a long collision region and multi (about 200)-bunch collisions.

Finally, the expected fluctuation in X-ray yield is less than 10%.

3. Applications

Among the anticipated uses of monochromatic hard X-

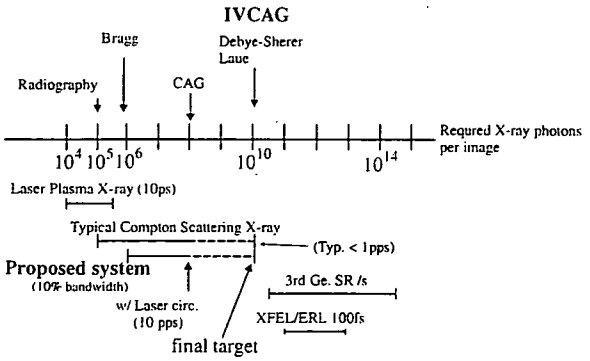

Fig. 12. Summary of required X-ray photons for various applications and X-ray yield of various X-ray sources.

rays of 10–50 keV include marked improvements not only in dynamic IVCAG but also monochromatic CT, monochromatic X-ray imaging, K-edge imaging, and protein crystallography. Required X-ray photons per image for X-ray imaging, crystallography, CAG and X-ray yield of various X-ray sources are summarized in Fig. 12.

Discussion and demonstration of advantages of narrow bandwidth X-ray beams have beem presented by Carroll.[16] A compact hard X-ray source with X-ray yield of 10^8 photons/s (10^7 photons/pulse) can be applied to X-ray imaging.

Advantages of the proposed system are intense (10^7 photons/pulse), narrow bandwidth (1 to 10 percent), and short pulse (1 μs) X-ray generation with high (10 pps) repetition rate. This means that the system can be applied to dynamic imaging. Ont the other hand, repetition rate of most high intensity X-ray sources based on Compton scattering is low (<1 pps) that is limited by the high power laser system. A dynamic CAG experiment on animals with localization of contrast agent by catheter will be performed using the proposed hard X-ray source.

4. Upgrade of the X-ray Yield

A 33 keV monochromatic X-ray with 10^{11} photons/s (10^9–10^{10} photons/shot) is required for IVCAG. 10^4 photons/pixel/image are needed to observe meaningful differences in artery with 5% contrast agent and other tissue. The required photons for a 10 cm × 10 cm image with 1 mm resolution are 10^8. The transmittance of X-rays in the human body of from 1 to 10% must be taken into account. Finally, 10^9 to 10^{10} photons/image of X-rays must be applied to a patient. To enhance the luminosity of laser-beam collisions, we adopt the technique of circulation of laser light shown in Fig. 13. The pulse length of a Q-switch Nd:YAG laser is shorter than the RF pulse length. This means that most electron bunches cannot collide with laser light. The laser pulse circulating system is effective to increase X-ray yield in the proposed system. The collided laser light is bent by a mirror and its polarization plane is changed by a Pockels cell. Passage of the laser light from the Q-switch laser system and circulated laser light are merged by a polarized beam splitter. Laser light can then collide with electron the beam again (see Fig. 14).

The total laser energy in the circulation I_N ($N = 1, 2, \ldots$: the times circulated) is

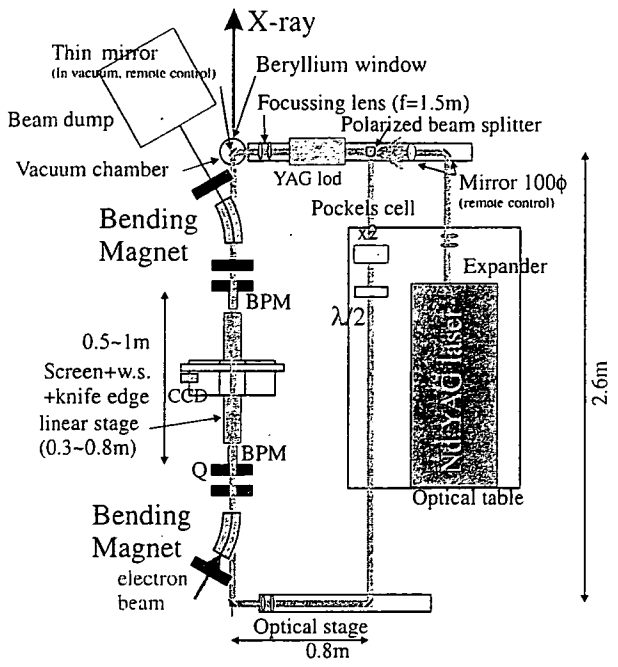

Fig. 13. Illustration of the laser pulse circulating system.

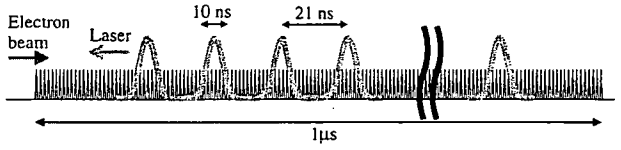

Fig. 14. Bunch structure of laser electron beams with laser circulating system.

$$I_N = \sum_{n=1}^{N} I_0 A^n = I_0 \frac{A - A^n}{1 - A} \tag{5}$$

where I_0 is the initial pulse energy of the laser pulse; A, the transmittance of the laser pulse per revolution on the circulation line; and n, the number of revolution. The laser pulse collides 20 times if the revolution time of the laser pulse is 50 ns. We expect the enhancement of X-ray yield by a factor of 10 times with 90% transmittance of the laser pulse per revolution in the laser circulation.

For the next step in the laser pulse circulating, we adopt YAG rod as a gain medium in the circulation line to compensate for the laser pulse energy loss in the line with a 5 J laser pulse, and the revolution time is reduce to 20 ns. The X-ray yield will reach 10^9 photons/pulse (total).

A high power (above 5 J/pulse) ring laser system is best to increase the X-ray yield in the proposed system. The ring laser system will be adopted to the X-ray source in the final step.

To achieve the 10^{11} photons/s required for dynamic IVCAG, the repetition rate must by increased to 50 pps. The intensity of the electron beam will be increased by understanding and controlling the beam loading, Wakefields in the RF gun and the accelerating structure.

5. Conclusion

We are developing a compact X-ray source using laser-electron collision based on an X-band linac for dynamic IVCAG. To realize a remarkably compact system, we adopted the X-band system and commercial Q-switch laser. We expect the X-ray yield to be 10^7 photons/pulse (10^8 photons/s). A beam line for proof-of-principle experiment is designed and intensity fluctuation of X-ray is expected to be under 10%. 10^8 photons/pulse (10^9 photons/s) will be realized by a laser circulation system without power loss compensation. The laser gain medium will be applied the laser circulation to up to 10^9 photons/pulse (10^{10} photons/s). Twenty eight percent of photons with an energy spread of 10% rms will be available by collimating the scattering angle of X-ray photons.

The final target shown in Fig. 2 will be realized and widely applied to the monochromatic X-ray imaging for medicine.

Acknowledgements

We would like to thank to Dr. Emeritus Y. Hirao, Dr. S. Yamada of NIRS and M. Seya of Ministry of the Education, Culture, Sports Science and Technology. We discussed and designed the thermionic-cathode X-band RF gun and X-band accelerations structure with Dr. M. Yamamoto, Mr. H. Sakae and Mr. K. Matsuo of IHI. Dr. S. Otsuka of Tsukuba University and Dr. K. Hyodo of KEK suggested and gave us the information on dynamic IVCAG. This study was performed under the national project of "Development of Advanced Compact Accelerators" by Ministry of Education, Culture, Sports, Science and Technology in Japan.

1) J. H. Hubbell and S. M. Seltzer: NISTIR 5632 (1995).
2) E. Rubenstein, R. Hofstadter R, H. D. Zeman, A. C. Thompson, J. N. Otis, G. S. Brown, J. C. Giancomini. H. J. Gordon, R. S. Kernoff, D. C. Harrison and W. Thomlinson: Proc. Natl. Acad. Sci. USA **83** (1986) 9724.
3) S. Ohtsuka, Y. Sugishita, T. Takeda, Y. Itai, J. Tada, K. Hyodo and M. Ando: Br. J. Radiol. **72** (1999) 24.
4) K. Dobashi, M. Uesaka, A. Fukasawa, H. Iijima, J. Urakawa, T. Higo, M. Akemoto and H. Hayano: Proc. 8th European Particle Accelerator Conference in Paris, France, 2002, p. 667.
5) M. Uesaka, A. Fukasawa, K. Dobashi, H. Iijima, J. Urakawa, T. Higo, M. Akemoto and H. Hayano: Proc. XXI Int. LINAC Conf. Gyeongju, Korea, 2002, p. 626.
6) A. Fukasawa, T. Kobayashi, M. Uesaka, J. Urakawa, T. Higo, M. Akemoto and H. Hayano: Proc. 2nd Asian Particle Accelerator Conf. 2001, p. 843.
7) A. Fukasawa, T. Kobayashi, M. Uesaka, J. Urakawa, T. Higo, M. Akemoto and H. Hayano: IJAEM **14** (2001/2002) 221.
8) GLC Project, KEK Report, 2003-7 (2003).
9) V. O. Klein and Y. Nishina: Z. Phys. **52** (1928) 853.
10) V. O. Klein and Y. Nishina: Z. Phys. **52** (1928) 869.
11) K. Yokoya; CAIN2.1e, private commutations.
12) K. Hirata: An introduction to SAD (Strategic Accelerator Design), Second Advanced ICFA Beam Dynamics Workshop, CERN 88-04, 1988.
13) A. Takeshita *et al.*: NIM PR A **421** (1999) 43.
14) K. Dobashi, M. Fukuda, T. Hirose, Y. Kamiya, I. Sakai, T. Aoki, A. Higurashi, T. Oshima, M. Washio, Y. Kurihara, T. Okugi, T. Omori and J. Urakawa: IJAEM **14** (2001/2002) 227.
15) K. Dobashi, M. Fukuda, T. Hirose, Y. Kamiya, I. Sakai, T. Aoki, A. Higurashi, T. Oshima, M. Washio, Y. Kurihara, T. Okugi, T. Omori and J. Urakawa: KEK Preprint 2001-64 (2001).
16) F. E. Carroll: Am. J. Roentgenology **179** (2002) 583.

Journal of the Korean Physical Society, Vol. 49, No. 1, July 2006, pp. 286~297

X-band Thermionic Cathode RF Gun and Multi-Beam Compton Scattering Monochromatic Tunable X-ray Source

Fumito SAKAMOTO,* Mitsuru UESAKA, Katsuhiro DOBASHI, Atsushi FUKASAWA and Tomohiko YAMAMOTO
Nuclear Professional School, The University of Tokyo 2-22 Shirakata-Shirane, Tokai, Naka, Ibaraki 319-1188, Japan

Junji URAKAWA, Toshiyasu HIGO and Mitsuo AKEMOTO
High Energy Accelerator Research Organization 1-1 Oho, Tsukuba, Ibaraki 305-0801, Japan

Kenichi MATSUO and Hisaharu SAKAE
Ishikawajima-Harima Heavy Industries Co., Ltd. 1 Shin-Nakahara, Isogo, Yokohama, Kanagawa 235-8501, Japan

Masashi YAMAMOTO
Akita National College of Technology 1-1 Iijima-Bunkyo, Akita, Akita 011-8511, Japan

(Received 25 January 2006)

A Compton scattering X-ray source consisting of an X-band (11.424 GHz) electron linear accelerator (linac) and Q-switched Nd:YAG laser is currently under construction. Monochromatic hard X-rays are required for a variety of medical and biological applications. The new hard X-ray source produces monochromatic X-rays via collision between a 35-MeV multi-bunch (10^4 bunches in a 1 μs RF pulse) electron beam and 1.4 J/10 ns (532 nm) Nd:YAG laser beam. The linac uses an X-band 3.5-cell thermionic cathode RF gun and an alpha magnet as an injector. The thermionic cathode RF gun is the first of its kind and can generate a high current (2 μA) and a multi-bunch 2-MeV electron beam. To increase the efficiency of the X-ray yield, a laser pulse circulation system is adopted, that can increase the X-ray intensity by up to 50 times. This scheme can produce monochromatic tunable X-rays (10 $\sim$ 40 keV) with intensities of $10^8 \sim 10^9$ photons/sec. In addition, the X-ray energy can be changed rapidly over 40 ms by two different wavelength lasers (YAG fundamental (1064 nm), 2nd harmonic (532 nm)) and an optical switch. This quick energy change is very important for living specimens and is very difficult to achieve in light sources such as a large SR (Synchrotron Radiation) source. The system can be used for dual-energy X-ray CT and subtraction X-ray CT to determine the 3D distribution of the atomic number density and electron density, and specified atomic distribution, respectively. In this paper, we describe the details of the system, report on experiments on the X-band thermionic cathode RF gun, and discuss applications of monochromatic X-rays.

PACS numbers: 29.27.Eg, 87.62.+n
Keywords: X-ray source, Compton scattering, X-band linac, X-band thermionic cathode RF gun

I. INTRODUCTION

X-rays of 10 $\sim$ 40 keV are of great use in medical science, biology, and material science. Example techniques that use such X-rays are dynamic intravenous coronary arteriography (IVCAG) [1,2] and monochromatic X-ray imaging. In addition, the techniques of dual energy X-ray CT [3] and subtraction imaging using a contrast agent and dual energy X-rays may be realized by using two monochromatic X-ray beams.

Intense hard X-rays are generated by third-generation light sources. However, most synchrotron radiation (SR) sources are too large to be widely used for monochromatic X-rays. Therefore, we are developing a compact monochromatic X-ray (10 $\sim$ 40 keV) source based on laser-electron collisions in an X-band (11.424 GHz) linear accelerator (linac) system [4–8] at the Nuclear Professional School, the University of Tokyo. Since the scattering angle of the photon depends on its energy, one to ten percent narrow-band X-rays are generated by collimating scattered photons.

In our system, a multi-bunch electron beam generated by a thermionic cathode RF gun is collimated and compressed temporally by an alpha magnet and

*E-mail: saka@nuclear.jp; uesaka@nuclear.jp;
Tel: +81-29-287-8413; Fax: +81-29-287-8488

Table 1. Performance of linac/laser Compton scattering X-ray sources.

Laboratory	Electron energy	Charge	Wavelength and energy of laser pulse	X-ray energy and intensity	Fluctuation of X-ray
SHI [16]	14 MeV (S-band)	400 pC Single bunch	800 nm, 300 mJ, (Ti:Sapphire, 300 ps)	3.5 keV $<10^4$ photons/shot	50 %
MXI Systems Inc [15]	25 MeV (S-band)	500 pC Single bunch	1 μm, 20 J (Nd:Glass)	12 ~ 50 keV 10^8 photons/sec	50 %
LLNL [17]	57 MeV (S-band)	250 pC Single bunch	780 nm, 400 mJ (Ti:Sapphire, fs)	40 ~ 80 keV 10^7 photons/sec	50 %
SLAC [18]	60 MeV (X-band)	500 pC Single bunch	800 nm, 300 mJ (Ti:Sapphire, fs)	20 ~ 85 keV 10^8 photons/sec	80 %
U. Tokyo/NIRS/KEK [5]	35 MeV (X-band)	20 pC × 10000 Multi-bunch	1 μm, 2 J, (Nd:YAG, 10 nsec)	33 keV 10^8 photons/sec	<10 %

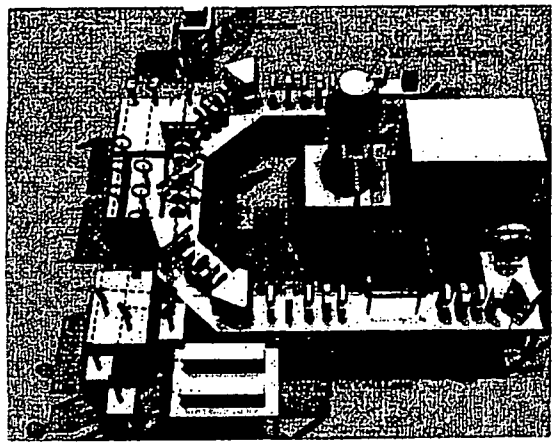

Fig. 1. Schematic of the compact X-ray source based on the X-band thermionic cathode RF-gun, and X-band accelerating structure and a Q-switched Nd:YAG laser.

accelerated by an X-band accelerating structure. The thermionic cathode RF gun can generate a high-current (2 μA) multi-bunch (10^4 bunches in 1 μs) electron beam. The experimentally confirmed energy of the electron beam generated by the RF gun is 2 MeV. The electron beam is bent by achromatic bends and focused at the collision point (CP). An approximately 10-ns hard X-ray is generated via Compton scattering upon laser-electron collision. This system can also generate dual energy monochromatic hard X-rays by using two Nd:YAG lasers. The laser system for Compton scattering is composed of a Q-switched Nd:YAG laser.

To demonstrate the proposed X-ray source, an X-band linac beam line (shown in Fig. 1) for a proof-of-principle experiment is under construction. The X-ray yield by the electron beam and a Q-switched Nd:YAG laser of 2.5 J/10 ns (1064 nm) is 10^7 photons/RF-pulse (10^8 photons/sec at 10 pps). A demonstration X-band beam line is being commissioned. We are also designing a laser circulation system [9] to increase the X-ray yield up to 10^8 photons/pulse (10^9 photons/sec).

In this paper, we present the design and numerical analysis of the demonstration X-ray source system. The first experimental verification of the X-band thermionic cathode RF gun is also described.

II. BRIEF REVIEW OF LINAC-LASER COMPTON SCATTERING X-RAY SOURCE

Early experimental demonstrations of proof-of-principle systems have been made at LBL [10,11], BNL [12], KEK-JAERI-U.Tokyo [13] and at other installations in the 1990s. The use and distribution of table-top Ti:Sapphire lasers, CO_2 lasers, Nd:Glass lasers and RF photoinjectors have contributed to the development of the systems. In particular, developments have recently allowed the second harmonic to be produced as well as the fundamental [14]. The existing systems are specialized for medical and bio-scientific uses, such as for monochromatic X-ray imaging, dual-energy X-ray CT, subtraction X-ray CT, angiography, Auger cascade therapy, protein structural analysis, *etc.* These systems are summarized in Table 1. Of particular note is the pioneering work on medical monochromatic X-ray imaging performed by Carroll *et al.* [15]. Most system use scattering between a single electron bunch and a single laser pulse and hence cannot achieve X-ray intensities as high as 10^8 photons/sec [16–18]. Dynamic imaging, angiography and protein structural analysis are difficult without a high intensity. To address this problem, multiple scattering between multi-electron-bunches and multi-laser-pulses could be employed to generate an X-ray intensity of more than 10^9 photons/sec.

We define here the first and second generation of scattering in X-ray sources. The first generation established the following:

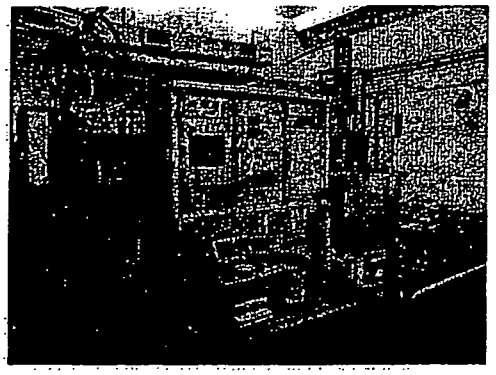

Fig. 2. Klystron and modulator (Toshiba E3768A).

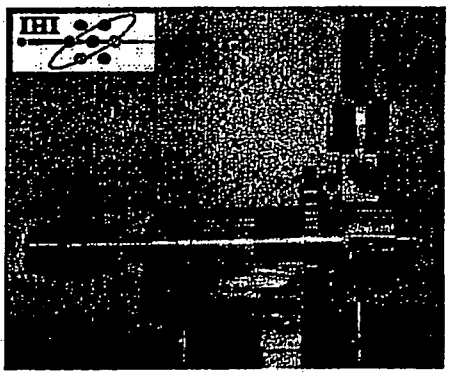

Fig. 3. X-band thermionic cathode RF gun (Ishikawajima-Harima Heavy Industry Co., Ltd).

- First demonstration and application,
- Intensity up to 10^8 photons/sec,
- Intensity fluctuation due to time-jitter between electron beam and laser pulses.

The second generation will realize the following:

- Multi-scattering of electron beam and laser pulses,
- Intensity of more than 10^9 photons/sec,
- Variety of applications in medicine, protein structural analysis, nondestructive evaluation, and nuclear engineering.

In this paper, we report on the development a typical second-generation system underway at the University of Tokyo. We note that, KEK is developing a multi-bunch S-band photoinjector for the Global Linear Collider, which can produce more than 100 nC per RF pulse [19]. This system may be a second candidate for the second-generation source.

III. COMPTON SCATTERING X-RAY SOURCE BASED ON X-BAND LINAC

We detail here a compact X-ray source based on the proposed X-band linac shown in Fig. 1. A multi-bunch electron beam generated by a thermionic cathode RF gun is accelerated by an X-band accelerating structure. The beam is bent and focused at the collision point. Approximately 10 ns X-rays are generated via Compton scattering on laser-electron collision.

1. X-band Linac

An X-band linac is used with the compact hard X-ray source. The RF wavelength of the X-band is 1/4 of the S-band (2.856 GHz). However, the maximum field gradient of ~40 MV/m gives remarkable compactness.

A 0.7-m long X-band accelerating structure is used for the X-ray source. The X-band accelerating structure technology developed for future linear colliders [19] at KEK and Stanford Linear Accelerator Center (SLAC) are fully adopted for this system. Initially, the Round Detuned Structure (RDS) is to be adopted and is already being manufacturing.

Table 2. Beam parameters at collision point.

Beam energy	35 MeV
Charge/bunch	20 pC
Bunches/RF pulse	10^4
Beam size (rms) (x,y)	100, 100 μm
Normalized emittance (rms) (x, y)	10, 10 πmm-mrad

We adopt a Periodic Permanent Magnet (PPM) type X-band klystron (Toshiba E3768A) designed for linear colliders [20]. The klystron modulator is being designed to fit the X-ray source. The nominal RF power is above 50 MW in 1 μs.

The beam optics of the X-band linac beam line were designed using SAD (Strategic Accelerator Design) [21] code. Photographs of the klystron/modulator are shown in Fig. 2. The beam parameters at the collision point (CP) are shown in Table 2.

2. 3.5-cell X-band Thermionic Cathode RF Gun

The injector of the system consists of an X-band thermionic cathode RF gun and an alpha magnet. The inner slit of the alpha magnet is used to eliminate low-energy particles. It is also used as a bunch compressor. Fig. 3 shows the X-band thermionic cathode RF gun. The detailed design and manufacture were performed by Ishikawajima-Harima Heavy Industries Co., Ltd. (IHI). The cavity of the RF gun has three full cells and a half cell (see Fig. 4) and is operated at 11.424 GHz in the π mode. The nominal beam energy is 2 MeV. A coaxial coupler [22] is introduced to ensure axial symmetry of the field in the gun and for placement inside a solenoid coil. The thermionic cathode is a dispenser type, and

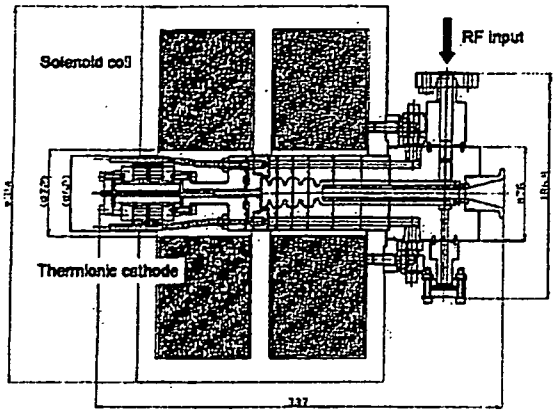

Fig. 4. Cut-away view of the X-band thermionic cathode RF gun cavity.

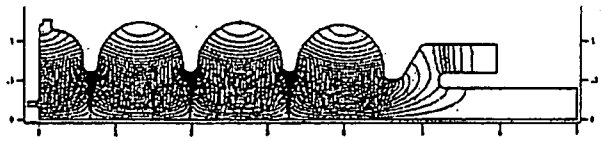

Fig. 5. Electric field of the 3.5-cell X-band thermionic cathode RF gun. Red lines show the rH_ϕ contours.

the material is tungsten. The edge of the cathode is manufactured to reduce the radius size R to avoid concentration of the electric field at the edge. Tuning of the cavity can be controlled by moving the cathode position with a cathode plug. The thermionic cathode is operated at a current density of 20 A/cm^2, and its temperature is about 1000 °C. The radius of the effective emission area is 1.4 mm, hence, the output current is 1.23 A. Emission continues during the accelerating phase, that is 180°, and the emission rate is constant under a high voltage. The charge emitted in a RF period is given by

$$Q_{emit} = \frac{1}{2}\frac{\pi r_{cath}^2 \phi}{f_{RF}}, \tag{1}$$

where r_{cath} is the radius of the effective emission area, ϕ is the flux of the cathode current, and f_{RF} is the RF frequency in the cavity. In our case, the charge per bunch is 53.9 pC. The other properties of the cavity were calculated by using SUPERFISH [23]. The contour lines rH_ϕ of the field in the cavity are shown in Fig. 5 and the properties of the cavity are listed in Table 3.

Since the energy spread after the main acceleration must be less than 1 %, beams from the injector must satisfy the following relation:

$$\delta = \frac{\Delta E_{inj} + E_{acc}\Delta\phi_{inj}^2}{E} < 0.01, \tag{2}$$

where ΔE_{inj} is the energy spread at the injector, $\Delta\phi_{inj}$ is the bunch length in radians, and E_{acc} is the energy

Table 3. Properties of the 3.5-cell gun cavity, calculated by using SUPERFISH.

Resonant frequency	11.424 GHz
Transit time factor	0.703
Shunt impedance	2.46 MΩ
Q value	9350
Wake loss parameter	7.72 V/pC

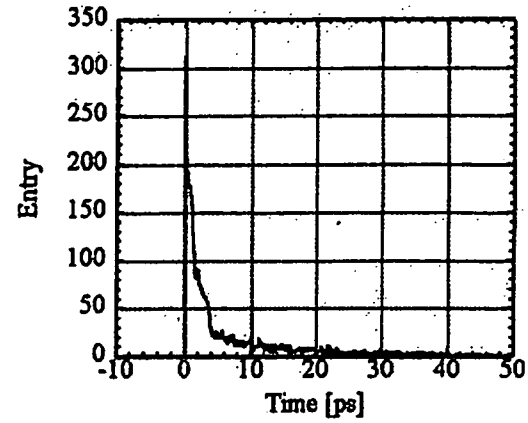

Fig. 6. Bunch form before the alpha magnet (simulation).

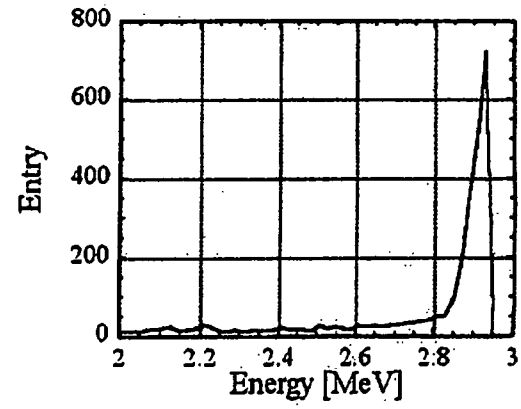

Fig. 7. Energy spectrum before the alpha magnet (simulation).

gain in the main accelerating structure. The dynamics of the particles in the gun cavity were simulated by using PARMELA [24]. The total charge was found to be 41 pC. The bunch length was 4.4 ps, and the energy spread was 0.16 MeV (rms over 2.25-MeV particles) (Figs. 6 and 7). The field gradient on the cathode surface is about 140 MV/m. Since δ becomes 0.01, lower particles should be eliminated. As Fig. 8 shows, when particles of energy less than 2.8 MeV are cut-off, the bunch satisfies the energy spread condition.

Table 4. Bunch parameters after the alpha magnet (simulation results).

Position of slit	121 mm	122 mm
Charge	20.2 pC	7.5 pC
Energy	2.92 ± 0.02 MeV	2.94 ± 0.01 MeV
Cut-off energy	2.86	2.91
Normalized emittance	15.1, 6.3 πmm-mrad	10.2, 4.1 πmm-mrad
Bunch length	2.2 ps	1.0 ps
δ	0.024	0.005

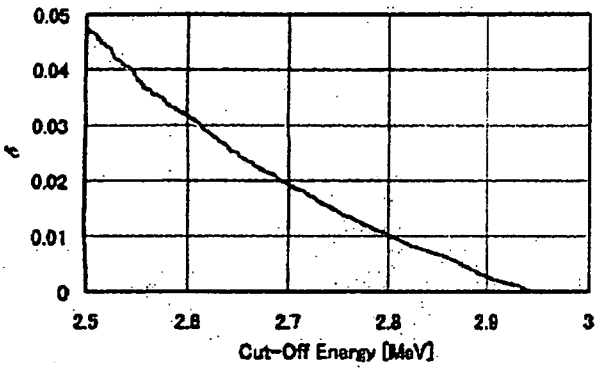

Fig. 8. Relation between the cut-off energy and the estimated energy spread after main acceleration (simulation).

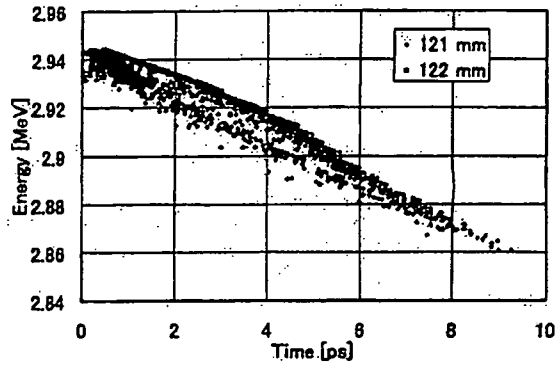

Fig. 9. Particle distribution in time-energy space. The blue dots are for a slit position of 121 mm, and the red dots are for 122 mm (simulation).

Next, the motion in the alpha magnet was calculated. The alpha magnet features a slit to cut out low-energy particles. By moving this slit, the cut-off energy can be controlled. Fig. 9 shows the particle distribution in time-energy space for different slit positions. The bunch parameters after the alpha magnet are listed in Table 4. When the slit position is 121 mm, the condition is not satisfied. It is satisfied for 122 mm, though the charge becomes small. The cut-off energy is higher than that previously estimated. This is because over bunching occurs in the alpha magnet, increasing the bunch length. To obtain the best compression and a high charge, the field gradient in the alpha magnet has to be higher. However, since it is difficult to increase the field, the energy should be decreased.

3. Laser System

Concentrating on the R&D of the accelerator, we chose a commercial and reliable laser for laser-electron collision. To realize a compact system, we used two Q-switched Nd:YAG lasers with an intensity of 2.5 J/pulse (1.4 J/pulse for the second harmonic), a repetition rate of 10 pps, a pulse duration of 10 ns (FWHM), and a wavelength of 1064 nm (fundamental).

In the second step, immediately switching the X-ray energy, we added a second laser system. The laser systems for the fundamental and the second harmonics are fired in turn. In this way, we can generate dual energy monochromatic X-rays with a repetition rate of 12.5 Hz (if the repetition rate of the linac is 25 Hz), as shown in Fig. 10. The advantage of this dual energy X-ray generation system is that the switching of the X-ray energy with a high repetition rate is very useful for dynamic subtraction imaging and dual energy X-ray CT. To increase

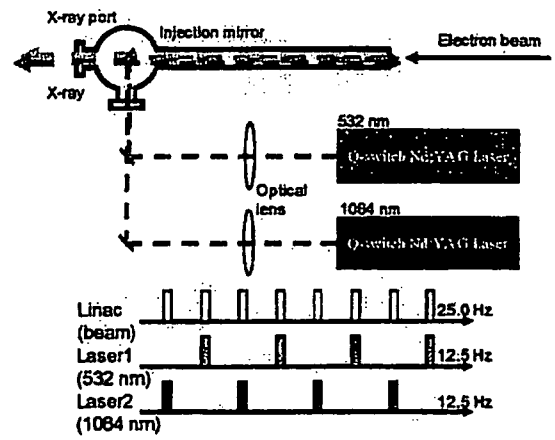

Fig. 10. Concept of the dual energy X-ray generation system.

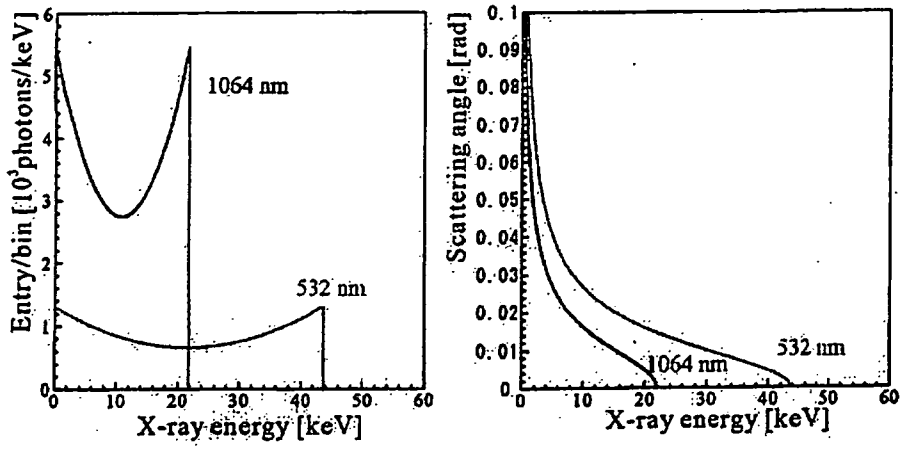

Fig. 11. Energy spectrum of X-rays for laser wavelengths of 1064 nm and 532 nm with an electron energy of 35 MeV.

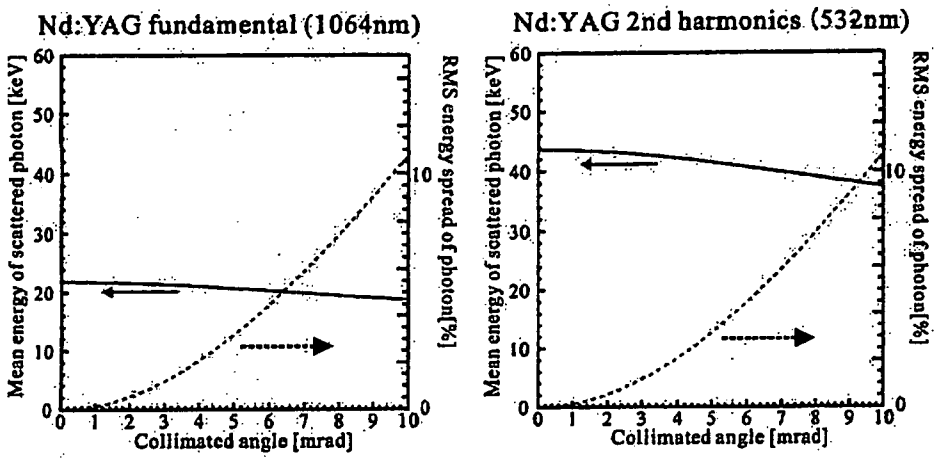

Fig. 12. Energy spread in the rms and the mean energies of available X-rays for each collimated angle.

Table 5. Properties of the X-rays generated with electron beam energy of 35 MeV and charge of 20 pC/bunch.

Laser wavelength	1064 nm	532 nm.
Pulse energy of laser (J/pulse)	2.5	1.4
X-ray yield (photons/sec)	1.0×10^9	4.4×10^8
Cut-off energy (keV)	2.86	2.91
Maximum X-ray energy (keV)	21.9	43.8

the X-ray yield, we need to design a technique for the circulation of the laser pulse to enhance the luminosity by 10 times.

4. X-ray Yield and Properties

The X-ray yield per bunch is calculated from the cross section of Compton scattering and the luminosity. The energy distribution and the relationship between the energy and the scattering angle of the X-ray for each laser wavelength with electron beam energy of 35 MeV are shown in Fig. 11. The properties of the X-rays are summarized in Table 5. Fig. 12 shows the mean energy and the rms energy spread of the available X-rays for each laser wavelength as functions of the scattered photons collimation angle.

IV. TEST OF THE X-BAND RF SOURCE AND THE X-BAND THERMIONIC CATHODE RF GUN

1. High-power Generation and RF Conditioning of the X-band RF Source

RF conditioning is required for the RF windows and circuit components, such as the RF waveguides. The ex-

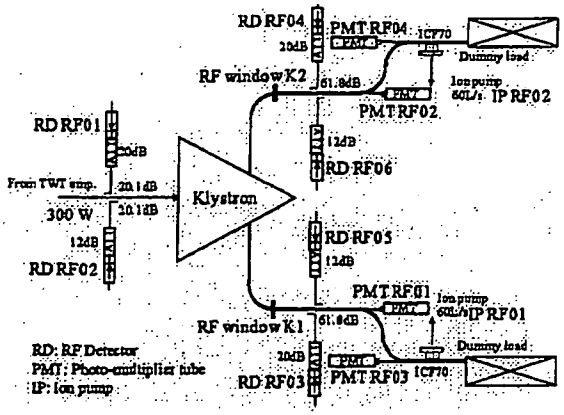

Fig. 13. Experimental setup of RF conditioning.

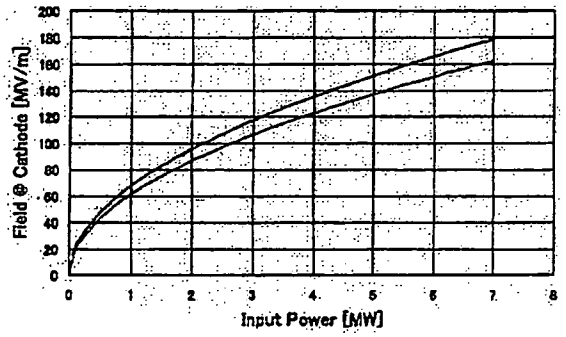

Fig. 14. Relation between the input RF power and the field gradient on the cathode surface.

perimental setup of the RF conditioning for the X-band klystron and waveguides is shown in Fig. 13. A low-level RF power of 300 W is fed to the klystron. This input power can be controlled by using a variable attenuator located just before the klystron input port. In order to reduce the load of the RF windows, the klystron has two output ports. The RF is damped by the dummy loads. Photo-multiplier tubes (PMT) are set to observe the light of the breakdown at the RF windows and dummy loads. The RF waveform is observed by using RF detectors at directional couplers. These signals are guided to a fast interlock system that stops the RF within 400 ns. The reflection signal from the dummy load is also used for the interlock.

The goal of the RF conditioning is to achieve 50 MW and 1 μs. However, the conditioning takes a long time. Therefore, we set a goal for an achievable level for the RF gun experiment. As Fig. 14 shows, 5 MW is required to make a field gradient of 140 MV/m at the cathode surface. Taking into account the loss around the circuit, we set a goal of 10 MW for each port (a total of 20 MW). The time structure of the electric field in the cavity is shown in Fig. 15. The target of the RF conditioning is 400 ns to fill the RF in the cavity. We have carried

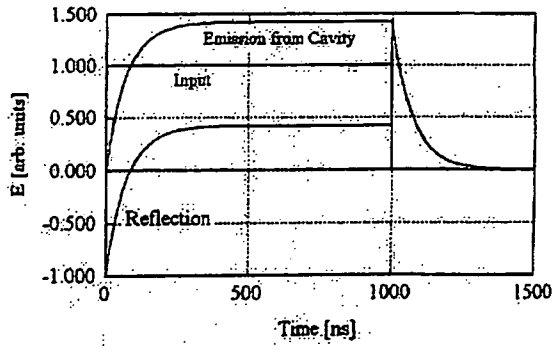

Fig. 15. RF waveform in the gun cavity.

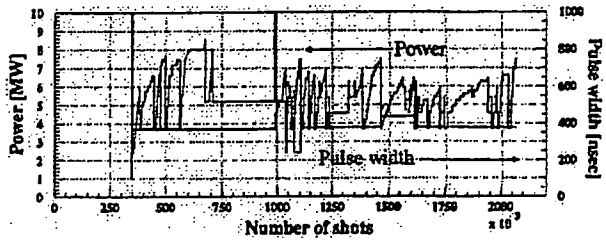

Fig. 16. Example of RF processing of an X-band klystron. The abscissa indicates the number of shots of the klystron under 10-Hz operation.

out RF conditioning and have achieved a total output power of about 20 MW and a pulse width of about 400 ns under 10-Hz operation. The total operation time was about 800 hours. Fig. 16 shows an example history of RF processing.

2. High-power Experiment of the X-band Thermionic Cathode RF Gun

As mentioned above, we have achieved sufficient power and pulse width to perform an RF gun experiment. For the beam generation experiment, we constructed the beam line shown in Fig. 17. This beam line includes an X-band thermionic cathode RF gun with a solenoid coil, an alpha magnet, quadrupole magnets, and a beam diagnostics section. The alpha magnet acts as an energy selector with its inner slits. Bunch compression and beam energy estimation are also expected to occur there. To observe a beam current from the RF gun, we set current transformers (CT) at the entrance and the exit of the alpha magnet. These current transformers are also used to estimate the beam energy.

Before starting the high-power feed, we measured the return reflection from the cavity to adjust the tuning of the cavity. In order to find the lowest reflection from the cavity, we carried out frequency scanning and evaluated the return loss as a function of the frequency. The minimum return loss was observed at 11.42450 GHz (Fig.

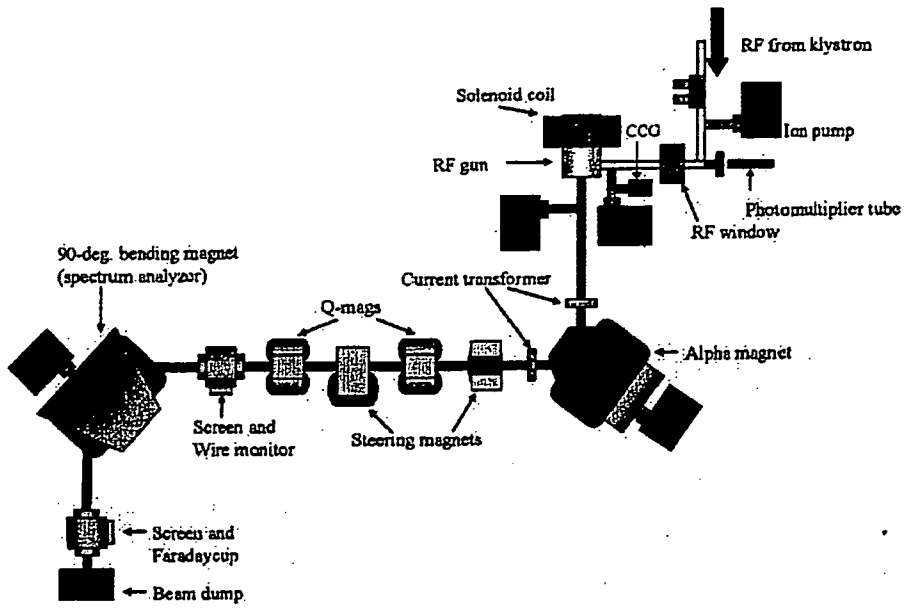

Fig. 17. Schematic view of test beam line for the X-band thermionic cathode RF gun.

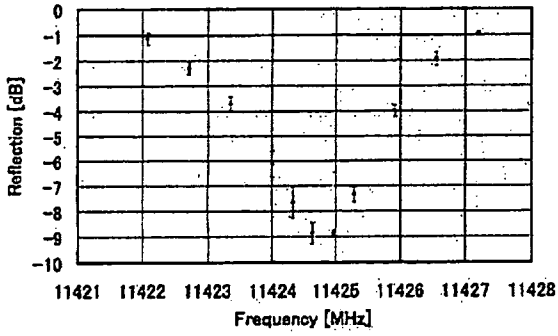

Fig. 18. Return loss at the gun cavity.

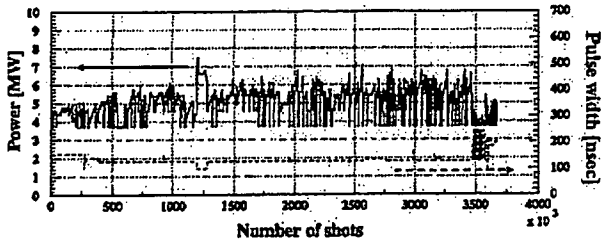

Fig. 19. Example of processing history of the X-band thermionic cathode RF gun. The abscissa indicates the number of shots of the klystron under 10-Hz operation. The solid line shows the output RF power, and the dotted line shows the pulse width of the RF.

18).

We started the RF conditioning of the RF gun cavity in April 2005. An example of the processing history is shown in Fig. 19. The total number of accumulated

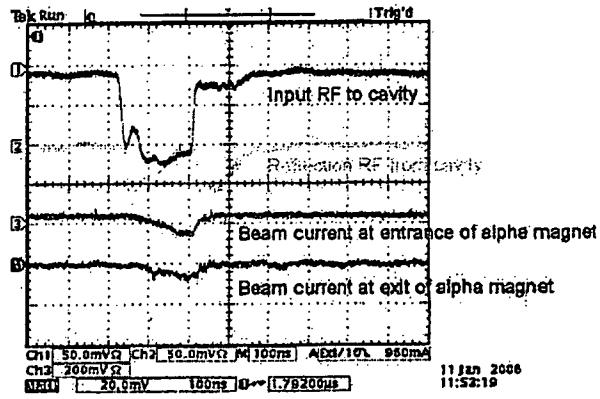

Fig. 20. RF waveform propagating forward and reflected (upper two lines) from the gun cavity. The bottom two lines show the beam currents observed at the entrance and the exit of the alpha magnet, by a current transformer.

pulses was about 47×10^6 pulses. The maximum power and pulse width were 6 MW and 200 ns, respectively. The repetition rate was 10 Hz. Typical RF waveforms propagating forward and backward under 6 MW and 200 ns are shown in Fig. 20. The forward propagating RF has a spike. Since there are no circulators that can sustain high power at X-band frequencies, the reflected pulse returns to the klystron directly and back to the gun cavity, again affecting the forward pulse. The beam current signals observed by the current transformers are also included in Fig. 20. The beam current from the cavity is 0.15 μA. The beam energy was measured by using the alpha magnet and the current transformer. The princi-

Table 6. Experimental results of the beam generation experiment of the X-band thermionic cathode RF gun.

Beam energy	2 MeV (<10 %)
Beam current (after alpha magnet)	0.15 μA (0.01 μA)
Charge/bunch (after alpha magnet)	~1 pC/bunch (~0.1 pC/bunch)
RF input power	6 MW
RF pulse width	200 nsec

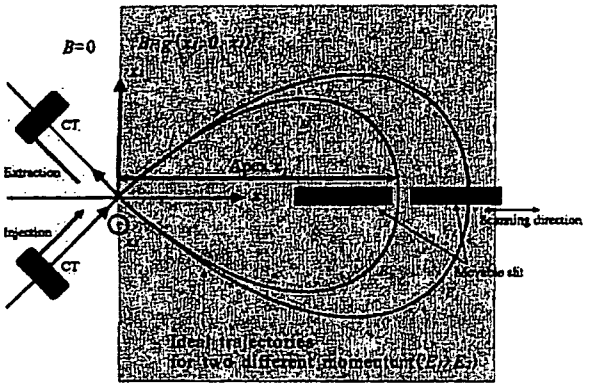

Fig. 21. Beam energy measurement by an alpha magnet.

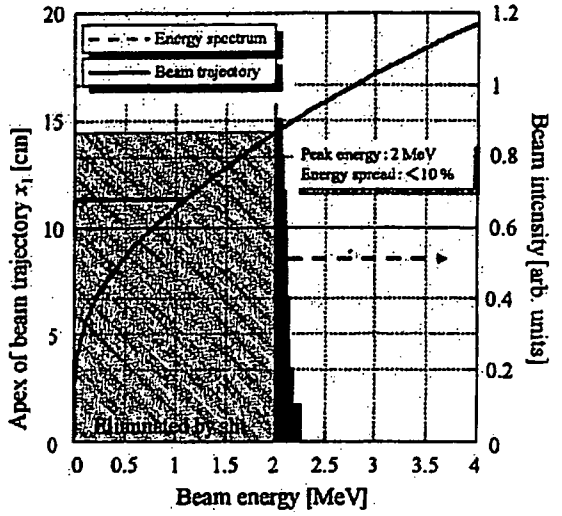

Fig. 22. Energy spectrum of the electron beam measured by the alpha magnet (right-hand axis). The left-hand axis shows the apex of the beam trajectory in the alpha magnet.

ple of the energy measurement using the alpha magnet is illustrated in Fig. 21. The ideal trajectory of a charged particle in the alpha magnet is determined by the field gradient of the alpha magnet and the kinetic energy of the charged particle. The energy spectrum is estimated by using the inner slit of the alpha magnet to observe the transmission of the beam current. Fig. 22 shows the energy spectrum of the electron beam measured by using the alpha magnet. The peak energy is 2 MeV, and the energy spread is less than 10 %. The lower-energy components are eliminated by the inside tungsten plate of the slit. The observed beam parameters are summarized in Table 6. The nominal beam current and the charge per bunch are 2 μA and 20 pC/bunch, respectively. However, the measured parameters are not consistent with the nominal values. This is due to that fact that the pulse width cannot be extended over the cavity filling time. Breakdown frequently occurred in the gun cavity. The location and the breakdown factor are being investigated. Precise diagnostics of the electron beam, such as the emittance and the bunch duration, will be carried out in the future.

V. DUAL-ENERGY X-RAY CT

The effective atomic number Z_{eff} and the electron density ρ_e of a material can be obtained by using the linear attenuation coefficients using for different energy monochromatic X-rays. The linear attenuation coefficient μ of a material can be approximately written as a function of the atomic number Z and the X-ray energy E by using a formula proposed by Jackson and Hawkes [25],

$$\mu(Z,E) \cong \rho\frac{N_A}{A}Z\left\{2\sqrt{2}Z^4\alpha^4\left(\frac{mc^2}{E}\right)\phi_0\sum_{u'}f_n u' + \sigma_{KN} + \frac{Z(1-Z^{b-1})}{Z\gamma^2}\sigma_{SC}^{coh}(Z',E')\right\} = \rho_e(Z^4F(Z,E)+G(Z,E)), \quad (3)$$

where ρ is the mass density, N_A is Avogadoro's number, A is the atomic mass, $f_n u'$ is a collection terms for the photoelectric absorption cross section, σ_{KN} is the Klein-Nishina cross section, and σ_{SC}^{coh} is the coherent scattering cross section of the standard element Z' at an energy of $E' = (Z'/Z)^{1/3}E$. A value of 0.5 has been proposed for the parameter b in the equation, and the standard element is taken to be oxygen [25]. If the linear attenuation coefficient is measured at two energies E_1 and E_2, the effective atomic number Z_{eff} and the electron density ρ_e can be derived by solving the following equations:

$$Z^4 = \frac{\mu(E_2)G(Z,E_1) - \mu(E_1)G(Z,E_2)}{\mu(E_1)G(Z,E_2) - \mu(E_2)G(Z,E_1)},$$

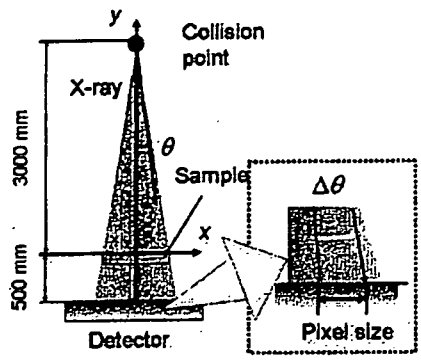

Fig. 23. Schematic drawing of the dual-energy X-ray CT system.

$$\rho_e = \frac{\mu(E_1)G(Z,E_2) - \mu(E_2)G(Z,E_1)}{F(Z,E_2)G(Z,E_1) - F(Z,E_1)G(Z,E_2)}. \quad (4)$$

The effective atomic number Z_{eff} is defined for a compound or a mixture as

$$Z_{eff} = \left(\sum_i q_i Z_i^k\right)^{1/k}, \quad (5)$$

where q_i is the fractional electron content of the i-th element in the compound or mixture, and $k = 4$.

This dual-energy method is limited in that Eq. (3) cannot be applied below the K-edge energy of a material. We will operate the compact X-ray source with an electron beam energy of 35 MeV and laser wavelengths of 1064 nm and 532 nm. In this case, the maximum X-ray energies are 21.9 keV and 43.8 keV, which should allow us to identify elements up to $Z = 38$. The energy spread $\Delta E/E$ of the monochromatic X-rays generated by SR is of the order of 10^{-4}, but the energy spread in the compact X-ray source is expected to be 1 to 10 % (rms), depending on the collimator angle [5]. The energy spread of X-rays is negligible with SR light sources, but for a Compton scattering X-ray sources the energy spread affects the accuracy of the atomic number identification.

To examine the applicability of dual-energy X-ray CT with the compact X-ray source, we performed a numerical simulation for low to medium Z elements ($Z \leq 38$). We use the linear attenuation coefficients of the materials listed in the photon cross section database [26] in the simulation. The geometry of the dual-energy X-ray CT system is shown in Fig. 23. We assume a point light source and a thickness and width of the sample of 1 mm and 20 mm, respectively. In this case, X-ray photons are collimated at 3.3 mrad. We note that the X-ray energy of the Compton scattering X-ray source depends on the scattering angle. Thus, the X-ray energy is unique at each pixel of the 2D detector. When the pixel size is 0.5 mm, $\Delta\theta$ is less than 0.2 mrad, and the energy spread on a pixel is in the order of 0.1 %. This small energy spread

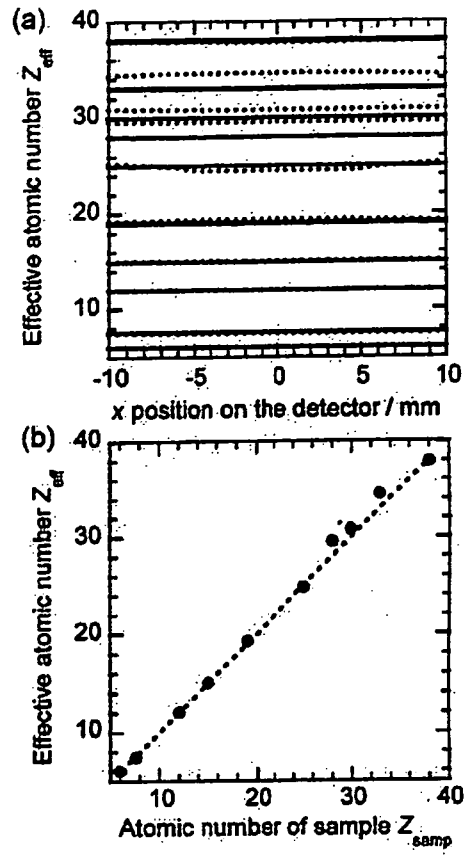

Fig. 24. Calculation results of dual-energy X-ray CT. (a) effective atomic number of each pixel for a spot size of 0.5 × 0.5 mm^2, and (b) average effective atomic number.

on a pixel should improve the accuracy of the dual-energy analysis. The effective atomic numbers obtained by using the linear attenuation coefficients for two energies on each pixel of the detector are shown in Fig. 24(a). The average of the effective atomic number Z_{eff} is plotted as a function of the atomic number of the sample Z_{samp} in Fig. 24(b). The accuracy of the estimated effective atomic number, $\Delta Z/Z$, is less than 3 % (rms), except for $Z = 25$ and 33. Hence, we have confirmed that the atomic number can be identified up to $Z = 38$ by using 21.9-keV and 43.8-keV X-rays with sufficient accuracy even with an energy spread of monochromatic X-rays of $1 \sim 10$ %.

VI. SYNERGY OF THE DRUG DELIVERY SYSTEM AND PHYSICAL ENERGIES

The synergy of the drug delivery system (DDS) and physical energies is becoming very important, following the development of genome/protein structural anal-

ysis and molecular imaging. Physical energies are high-energy radiation (X-rays, particles), visible lasers, and microwaves (RF). These energies enable cancer therapy without surgery, adverse effects, and heavy irradiation. The development of a new dendrimer-like DDS that can react with X-rays will allow photo-dynamic therapy not only for superficial organs, but for organs deeper in a human body. Iodine delivered and attached to the DNA of cancer cells can absorb 33.2-keV X-rays and emit electrons and several characteristic X-rays. This so-called cascade radiation can kill the DNA of nearby cancer cells. Such approaches may realize a radiation-assisted DDS in the near future. Nano-magnetic particles can now be effectively delivered to diseased body parts that can be well imaged by MRI, and several improvements to the technique are under development.

Large and medium-scale simulations are extremely important for this synergy work. It is important that the flow, diffusion, pharmaceutical chemistry, radiation chemistry *etc.* for DDS be numerically analyzed.

VII. CONCLUSION

We are currently developing a compact X-ray source based on laser-electron collision. To realize a compact system, we adopt an X-band linac and a commercial Q-switched laser. The X-ray yield from an electron beam and a Q-switched Nd:YAG laser of 2.5 J/10 ns is 10^7 photons/RF-pulse (10^8 photons/sec for 10 pps). We are also designing a technique of laser circulation to increase the X-ray yield up to 10^8 photons/pulse (10^9 photons/sec). So far, we have achieved beam generation from an X-band thermionic cathode RF gun. The beam energy is 2 MeV, and the energy spread is less than 10 %. This experimental high energy ($\sim$2 MeV) beam generation from the X-band thermionic cathode RF gun is the first such achievement. However, due to breakdown in the RF gun cavity, the beam current is about 1/10 of the nominal value. We are now investigating the reasons behind the breakdown in the cavity. Precise beam-diagnostic experiments on the emittance and the bunch duration are also being planned. In addition, preparations for the beam acceleration and laser system for Compton scattering are underway. We intend to start using Compton scattering monochromatic X-rays in medical applications in 2006.

ACKNOWLEDGMENTS

This work on developing the monochromatic hard X-ray source is performed under the national project of Development of Advanced Compact Accelerators in Japan and is partially supported by the Research Program on Development Innovative Technology (#0494) of the Japan Science and Technology Agency. The study of applications of the monochromatic X-ray source is supported by the Japanese Ministry of Education, Culture, Sports, Sciences and Technology and by the Japanese Ministry of Health, Labor and Welfare.

REFERENCES

[1] E. Rubenstein, R. Hofstadter R, H. D. Zeman, A. C. Thompson, J. N. Oits, G. S. Brown, J. C. Giancomini, H. J. Gordon, R. S. Kernoff, D. C. Harrison and W. Thomlinson, Proc. of National Academy Sci. USA **83**, 9724 (1986).

[2] S. Ohtsuka, Y. Sugishita, T. Takeda, Y. Itai, J. Tada, K. Hyodo and M. Ando, British Journal of Radiology **72**, 24 (1999).

[3] M. Torikoshi, T. Tsunoo, M. Endo, K. Noda, M. Kumada, S. Yamada, F. Soga and K. Hyodo, J. Biomedical Opt. **6**, 371 (2001).

[4] K. Dobashi, M. Uesaka, A. Fukasawa, H. Iijima, J. Urakawa, T. Higo, M. Akemoto and H. Hayano, Proc. of EPAC 2002, (France, 2002), p. 667.

[5] K. Dobashi, A. Fukasawa, M. Uesaka, H. Iijima, T. Imai, F. Sakamoto, F. Ebina, J. Urakawa, M. Akemoto, T. Higo and H. Hayano, Jpn. J. Appl. Phys. **44**, 1999 (2005).

[6] A. Fukasawa, T. Kobayashi, M. Uesaka, J. Urakawa, T. Higo, M. Akemoto and H. Hayano, Intern. J. Appl. Electromagnetism and Mechanics **14**, 221 (2001/2002).

[7] A. Fukasawa, M. Uesaka, F. Sakamoto, F. Ebina, K. Dobashi, J. Urakawa, M. Akemoto, T. Higo and H. Hayano, Nucl. Inst. Meth. B **241**, 921 (2005).

[8] M. Uesaka, A. Fukasawa, K. Dobashi, H. Iijima, J. Urakawa, T. Higo, M. Akemoto and H. Hayano, *Proc. of LINAC 2002*, (Gyeongju, 2002), p. 626.

[9] F. Ebina, A. Fukasawa, F. Sakamoto, H. Ogino, M. Uesaka and K. Dobashi, Nucl. Inst. Meth. B **241**, 905 (2005).

[10] E. Esarey, P. Sprangle, A. Ting and S. K. Ride, Nucl. Inst. Meth. A **331**, 545 (1993).

[11] K. J. Kim, S. Chattopadhyay and C. V. Shank, Nucl. Inst. Meth. A **341**, 351 (1994).

[12] I. V. Pogorelsky, I. Ben-Zvi, T. Hirose, S. Kashiwagi, V. Yakimenko, K. Kusche, P. Siddons, J. Skaritka, T. Kumita, A. Tsunemi, T. Omori, J. Urakawa, M. Washio, K. Yokoya, T. Okugi, Y. Liu, P. He and D. Cline, Phys. Rev. **ST-AB3**, 090702/1 (2000).

[13] M. Uesaka, H. Kotaki, K. Nakajima, H. Harano, K. Kinoshita, T. Watanabe, T. Ueda, K. Yoshii, M. Kando and H. Dewa, Nucl. Inst. Meth. A **455**, 90 (2000).

[14] M. Uesaka, Working Group D Summary of the Physics and Applications of High Brightness Electron Beam, (Italy, 2005).

[15] F. Carroll, Am. J. Rentgenol. **181**, 1197 (2003).

[16] M.Yorozu, J. Yang, Y. Okada, T. Yanagida, F. Sakai and A. Endo, Jpn. J. Appl. Phys. **40**, 4228 (2001).

[17] W. J. Brown, S. G. Anderson, C. P. J. Barty, S. M. Betts, R. Booth, J. K. Crane, R. R. Cross, D. N. Fittinghoff, D. J. Gibson, F. V. Hartemann, E. P. Hartouni, J. Kuba, G. P. Le Sage, D. R. Slaughter, A. M. Tremaine, A. J.

Wootton and P. T. Springer, Phys. Rev. ST. **7**, 060702 (2004).
[18] E. Vlieks, G. Caryotakis, D. Martin, C. A. DeStefano, W. J. Frederick J. Heritage and N. C. Luhmann, Jr., *Proc. of EPAC 2004* (Austria, 2004), p. 2837.
[19] K. Hirano, M. Fukuda, M. Takano, Y. Yamazaki, T. Muto, S. Araki, N. Terunuma, M. Kuriki, M. Akemoto, H. Hayano and J. Urakawa, Nucl. Inst. Meth. A **560-2**, 233 (2006).
[20] GLC report, KEK report 2003-7 (2003).
[21] K. Hirata, An introduction to SAD (Strategic Accelerator Design) Second Advanced ICFA Beam Dynamics Workshop, CERN 88-04 1988.
[22] F. B. Kiewiet, O. J. Luiten, G. J. H. Brussaard, J. I. M. Botman and M. J. Van Der Wiel, *Proceedings of EPAC 2000*, (Vienna, 2000), p. 1660.
[23] J. H. Billen, *Technical Report LLA-UR-96-1834, Los Alamos National Laboratory*, 1996.
[24] L. M. Young, Los Alamos National Laboratory report LA-UR-96-1834.
[25] D. F. Jackson and D. J. Hawkes, Phys. Rep. **70**, 169 (1981).
[26] XCOM http://physics.nist/gov/XCOM.

BEAM GENERATION AND ACCELERATION EXPERIMENTS OF X-BAND LINAC AND MONOCHROMATIC KEV X-RAY SOURCE OF THE UNIVERSITY OF TOKYO*

F. Sakamoto#, M. Uesaka, T. Yamamoto, T. Natsui and Y. Taniguchi, UTNS, Ibaraki, Japan
H. Sakae, D. Ishida, H. Nose. N. Kaneko and H. Sakai, IHI, Yokohama, Japan
T. Higo, M. Akemoto and J. Urakawa, KEK, Ibaraki, Japan
M. Yamamoto, Akita NCT, Akita, Japan

Abstract

In the Nuclear Professional School, the University of Tokyo (UTNS), we are constructing an X-band linear accelerator that consists of an X-band thermionic cathode RF gun and X-band accelerating structure. This system is considered for a compact inverse Compton scattering monochromatic X-ray source for the medical application. The injector of this system consists of the 3.5-cell coaxial RF feed coupler type X-band thermionic cathode RF gun and an alpha-magnet. The X-band accelerating structure is round detuned structure (RDS) type that developed for the future linear collider are fully adopted. So far, we have constructed the whole RF system and beam line for the X-band linac and achieved 2 MeV electron beam generation from the X-band thermionic cathode RF gun. In addition, we achieved 40 MW RF feeding to the accelerating structure. The laser system for the X-ray generation via Compton scattering was also constructed and evaluated its properties. In this paper, we will present the details of our system and progress of beam acceleration experiment and the performance of the laser system for the Compton scattering experiment.

INTRODUCTION

X-rays of 10-40 keV are great use in medical science, biology, and material science. Example techniques that are use such monochromatic X-rays are dual-energy X-ray CT [1] and subtraction imaging using a contrast agent and dual energy X-rays. These techniques may be realized by using two monochromatic X-ray beams.

Intense high energy (10-40 keV) X-rays are generated by the third-generation light source such as SPring-8, APS, and ESRF. However, most synchrotron radiation sources are too large to be widely used for monochromatic X-rays. One solution to realize a remarkable compactness is laser-electron collision (Compton scattering or Thomson scattering). Recently, many facilities are developing a Compton scattering X-ray source that consists of an electron linac and laser system [2-5]. However, most of them use the scattering between an ultra-short single electron bunch and an ultra-short single laser pulse to obtain short pulse X-ray beam. Therefore, they suffer a lack of X-ray intensity up to 10^8 photons/s and the fluctuation of the X-ray intensity due to the timing jitter between the electron bunch and the laser pulse. In order to overcome this weak point of Compton scattering X-ray source, one solution would be multiple scattering between multi-bunch electron beam and long-pulse laser beam. In the University of Tokyo, we are developing a more compact, high intensity, and high stable Compton scattering X-ray source. Our system consists of a 30 MeV X-band (11.424 GHz) multi-bunch electron linac and a Q-switch Nd: YAG laser (1.4 J/10 ns, 532 nm, second harmonic). In this paper, we describe the details of the high power and beam generation and acceleration experiment of the X-band linac with thermionic cathode RF gun and the details of the experimental setup for Compton scattering X-ray generation that are under construction.

* This work is performed under the national project of Development of Advanced Compact Accelerators in Japan and is partially supported by the Research Program on Development Innovative Technology (#0494) of the Japan Science and Technology Agency and in part supported by Health and Labour Sciences Research Grants.
#saka@nuclear.jp

X-BAND LINAC FOR INVERCE COMPTON SCATTERING X-RAY SOURCE AT THE UNIVERSITY OF TOKYO

Figure 1 shows schematic of the compact X-ray source at the University of Tokyo. Multi-bunch electron beam generated by a 3.5-cell X-band thermionic cathode RF gun, and is collimated and compressed by an alpha magnet, and accelerated by an X-band traveling type accelerating structure. The electron beam is bent by achromatic bends and focused at the collision point. The thermionic cathode RF gun can generate a high-current (2 μA) multi-bunch (10^4 bunches in 1 μs) electron beam. So far, we have achieved 2 MeV electron beam generation from the RF gun [6].

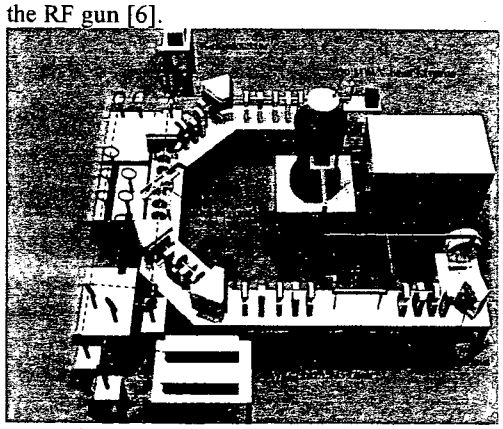

Figure 1: Schematic illustration of the compact Compton scattering X-ray source based on the X-band thermionic

cathode RF gun, X-band accelerating structure, and a Q-switch Nd: YAG laser at the University of Tokyo.

HIGH POWER TEST AND BEAM ACCELERATION EXPERIMENT OF X-BAND LINAC

The whole system of the RF system for the X-band thermionic RF electron injector and the X-band traveling wave accelerating structure is illustrated in Fig. 2. Low-level RF feed the RF about 300 W to the klystron. The variable attenuator that located at just before the klystron input port can control this input power. In order to reduce a load of the RF windows, there are two output ports at the klystron. Photo-multiplier tubes (PMT) are set to observe the light of breakdown on the RF windows and dummy loads. RF detectors at directional couplers observe the waveforms of the RF. These signals are guided to a fast interlock system. The fast interlock system stops the RF within 400 ns. Reflection signal from the dummy load is also used for the interlock. The RF pulses output from the klystron are combined by 3 dB hybrid and feed to beam line floor. The RF pulse is divided by 7 dB hybrid. In nominally, 40 MW and 6 MW with the pulse width of 1 μs are fed to the accelerating structure and the thermionic RF injector. In order to reduce the reflection from the RF gun cavity, we set 2.2 dB hybrid just after the 7 dB hybrid. So far, we have carried out the RF conditioning and achieved total output power about 40 MW and pulse width about 150 ns under 10 Hz operations. Figure 3 shows an example of history of RF processing. Figure 4 and 5 show the typical waveforms input to the accelerating structure and thermionic RF injector. The reason why the reflection waveform from the gun cavity seemed that the RF power is not filled in the cavity is due to the beam loading by emitted electron from the thermionic cathode.

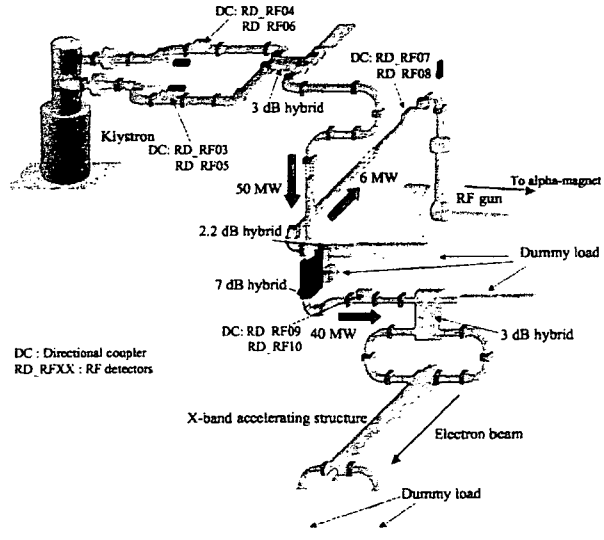

Figure 2: Schematic layout of the RF system for X-band thermionic RF injector and traveling wave accelerating structure.

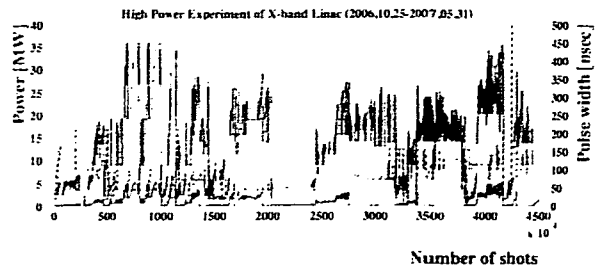

Figure 3: Example of the RF processing history. Red line shows RF power fed to accelerating structure, pink one is to the RF injector, and dotted blue line indicates the pulse width of the RF pulse.

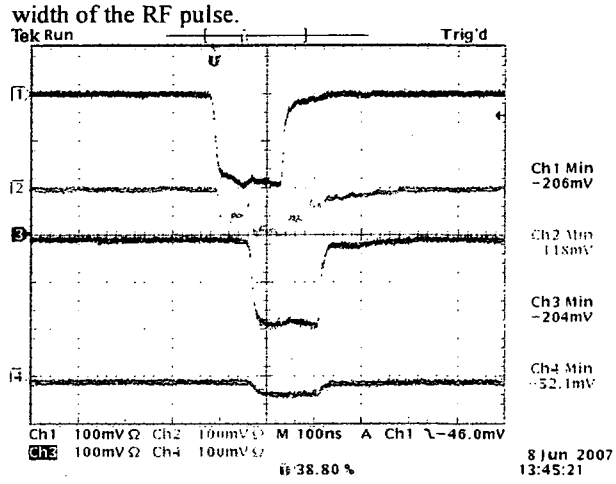

Figure 4: Typical waveform of RF pulse. (Ch.1: output from the klystron, Ch. 2 : reflection to klystron, Ch. 3: input to accelerating structure and Ch.4 :reflection from accelerating structure.

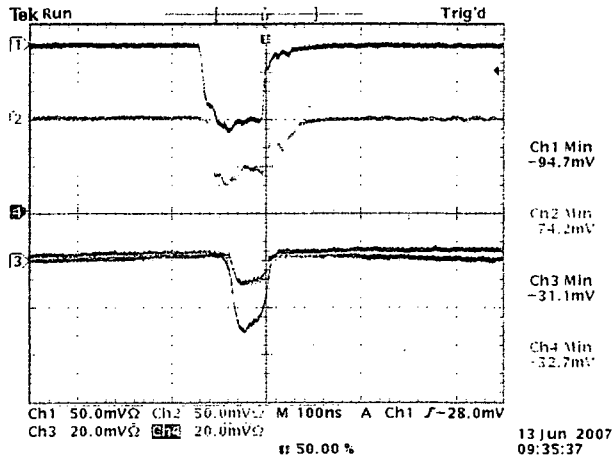

Figure 5: Typical waveform of RF pulse. (Ch.1: input to thermionic RF injector, Ch. 2: reflection from the injector, Ch. 3: beam current just after the alpha magnet and Ch. 4: beam current after the alpha-magnet.)

The beam optics for Compton scattering X-ray source were designed by using SAD (Strategic Accelerator Design) program [2,3]. After the alpha-magnet, the multi-bunch electron beam is passing trough quadruple

doublet and injects into the 0.5m accelerating structure. Figure 6 shows the beam profile at just after the accelerating structure. The beam energy is estimated about 22 MeV by using bending magnet.

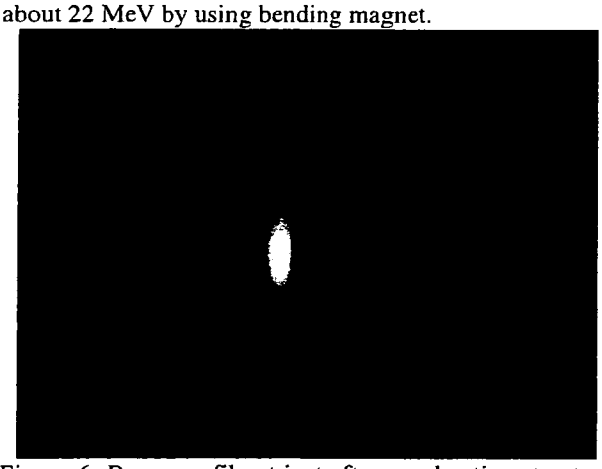

Figure 6: Beam profile at just after accelerating structure observed by luminescence screen. The energy of the electron beam is measured by bending magnet and is about 22 MeV,

EXPERIMENTAL SETUP FOR X-RAY GENERATION VIA COMPTON SCATTERING

For the next step, we are constructing a beam line of the X-band accelerating structure and Nd: YAG laser system for the X-ray generation via Compton scattering. Figure 7 shows the experimental setup for the Compton scattering. The X-band 0.5 m travelling-wave type accelerating structure accelerates the multi-bunch electron beam up to 30 MeV, and the beam is bent by achromatic bends and focused at the collision point. Since the laser pulse width, 10 ns (FWHM) is much shorter than the macro-pulse width of the electron beam (1 μs), we adopt a laser pulse circulation system [9,10]. Recently, we have carried out the measurement of the laser properties. The M^2 parameter is measured as 1.6 and 1.8 for horizontal and vertical, respectively. Figure 8 shows the stability of the laser pulse transverse beam size. The fluctuation of the beam size is with in 10 %. We will demonstrate the X-ray generation experiment via Compton scattering this July.

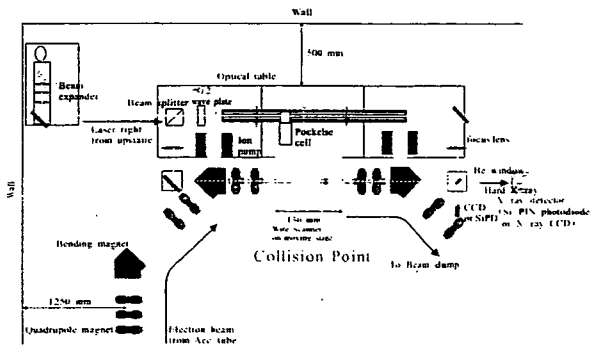

Figure 7: Experimental setup for X-ray generation via inverse Compton scattering at the University of Tokyo.

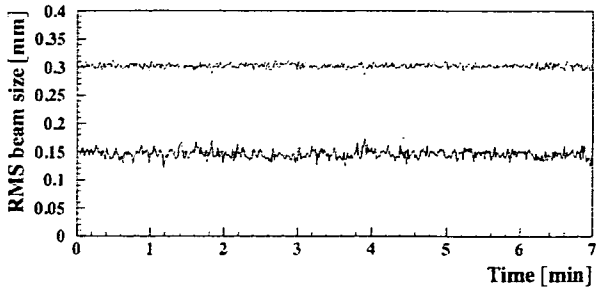

Figure 8: Stability of laser spot size at the collision point (top: horizontal, below: vertical).

SUMMARY

We are developing the compact, highly-intensity-, and highly-stable-Compton scattering X-ray source based on X-band multi-bunch electron linac and reliable Nd: YAG laser. So far, we have achieved the beam generation from the X-band thermionic cathode RF gun and carried out the beam acceleration experiment. The maximum beam energy is estimated about 22 MeV. This experimental high-energy multi-bunch beam generation and acceleration by the X-band thermionic cathode RF gun is the first achievement in the world. For the next stage, preparations for the beam acceleration and laser system for Compton scattering are underway. We will perform the experiments on the beam acceleration and the Compton scattering X-ray generation this October.

REFERENCES

[1] M. Torikoshi et. al., , *J. Biomedical Opt.* **6**, 371 (2001)

[2] R. Kuroda et. al., *Proc. of the European Particle Accelerator Conference*, Edinburgh, Scotland, (2006)

[3] F. Carroll, *Am. J. Rentgenol.* **181**. 1197 (2003)

[4] W. J. Brown, et. al., *Phys. Rev. ST.* 7, 060702 (2004)

[5] E. Vlieks, et. al., *Proc. of the European Particle Accelerator Conference*, Lucerne, Switzerland, (2004)

[6] F. Sakamoto, et. al., *J. Korean Phys. Soc.*, 49,1 (2006) 286.

[7] K. Dobashi, et. al., *Jpn. J. Appl. Phys.*, 44 (2005) 1999.

[8] K. Hirata, An introduction to SAD (Strategic Accelerator Design), Second Advanced ICFA Beam Dynamics Workshop, CERN 88-04, (1988)

[9] F. Ebina, et. al, *Nucl. Inst. and Meth.*, B 241 (2005) 905.

[10] H. Ogino, et. al., *J. Nucl. Sci. Technol.*, 43,21 (2006) 1458